The Crystal Structure of Spermidine/Spermine N^1-Acetyltransferase in Complex with Spermine Provides Insights into Substrate Binding and Catalysis[†,‡]

Eric J. Montemayor and David W. Hoffman*

Department of Chemistry and Biochemistry, Institute for Cellular and Molecular Biology, University of Texas, Austin, Texas 78712

Received December 27, 2007; Revised Manuscript Received June 24, 2008

ABSTRACT: The enzyme spermidine/spermine N^1-acetyltransferase (SSAT) catalyzes the transfer of acetyl groups from acetylcoenzyme A to spermidine and spermine, as part of a polyamine degradation pathway. This work describes the crystal structure of SSAT in complex with coenzyme A, with and without bound spermine. The complex with spermine provides a direct view of substrate binding by an SSAT and demonstrates structural plasticity near the active site of the enzyme. Associated water molecules bridge several of the intermolecular contacts between spermine and the enzyme and form a "proton wire" between the side chain of Glu92 and the N1 amine of spermine. A single water molecule can also be seen forming hydrogen bonds with the side chains of Glu92, Asp93, and the N4 amine of spermine. Site-directed mutation of Glu92 to glutamine had a detrimental effect on both substrate binding and catalysis and shifted the optimal pH for enzyme activity further into alkaline solution conditions, while mutation of Asp93 to asparagine affected both substrate binding and catalysis without changing the pH dependence of the enzyme. Considered together, the structural and kinetic data suggest that Glu92 functions as a catalytic base to drive an otherwise unfavorable deprotonation step at physiological pH.

Proper levels of the polyamines spermine and spermidine are essential for normal cell growth, and unusual levels of these polyamines have been associated with a variety of human diseases (*1–7*). The polyamine regulatory enzymes have therefore become attractive therapeutic drug targets (*8, 9*). Previous attempts to modulate cellular polyamines through attenuation of their biosynthesis have met limited success, and recent research has instead focused on the mechanism by which polyamines are removed from the cell (*10*). The reduction in levels of cellular polyamines is initiated by spermidine/spermine N^1-acetyltransferase (SSAT),[1] a highly regulated acetyltransferase that selectively acetylates the aminopropyl moieties of both spermine and spermidine (*11–15*). This acetylation step marks the polyamines for cellular export or oxidative degradation (*16–19*).

SSAT belongs to the GCN5-related *N*-acetyltransferase (GNAT) superfamily of acetyltransferases. This enzyme superfamily catalyzes the transfer of acyl groups from acetyl-CoA to the primary amines of various substrate molecules (*20*). Despite their low level of sequence homology, the GNAT proteins possess a conserved fold and are commonly found as homodimers in solution (*21*). The core of each protein monomer contains a mixed parallel/antiparallel β-sheet that is surrounded by a number of conserved α-helices. A splay between two parallel β-strands allows the positioning of the pantotheine moiety of acetyl-CoA near the enzyme active site. A β-bulge at the base of this splay is a conserved structural feature within the GNAT superfamily.

Various biochemical data support the notion of direct acyl transfer by the GNAT proteins, without the use of an acetylated enzyme intermediate (*22*). This type of acyl transfer requires the transient formation of a ternary complex of acetyl-CoA, the acyl acceptor substrate, and the enzyme. The primary amine of the acyl acceptor can initiate the chemical reaction through nucleophilic attack upon the carbonyl carbon of acetyl-CoA. The resulting bisubstrate intermediate can then decompose through proton transfer from a catalytic acid. Most members of the superfamily possess a tyrosine that is well-positioned to act as the catalytic acid (*20, 22–24*). The primary amine of an acceptor molecule is positively charged at physiological pH, so deprotonation is required before it can function as a nucleophile. This deprotonation can by driven by an active site amino acid, although numerous GNAT proteins appear to lack a residue appropriate for this role. Associated water molecules are thought to catalyze this deprotonation in the absence of an enzymatic base (*22, 25–27*).

Crystal structures of the human SSAT holoenzyme, a binary complex with acetyl-CoA, and a ternary complex with CoA and an inhibitor have previously been reported (*24*), as well as a complex with a bisubstrate inhibitor (*28*). This work describes the crystal structure of SSAT from mouse in complex with CoA, with and without bound spermine.

[†] This work was supported by Grant F-1353 from the Welch Foundation.

[‡] Coordinates for the crystal structure of mouse SSAT in complex with CoA and in complex with CoA and spermine have been deposited in the Protein Data Bank as entries 3bj7 and 3bj8, respectively.

* To whom correspondence should be addressed: Department of Chemistry and Biochemistry, Institute for Cellular and Molecular Biology, University of Texas, Austin, TX 78712. E-mail: dhoffman@mail.utexas.edu. Phone: (512) 471-7859. Fax: (512) 471-8696.

[1] Abbreviations: CoA, coenzyme A; BE-3-3-3, N^1,N^{11}-bis(ethyl)norspermine; GNAT, GCN5-related N^1-acetyltransferase; IPTG, isopropyl β-D-thiogalactopyranoside; NMR, nuclear magnetic resonance; PBS, phosphate-buffered saline; SDS−PAGE, sodium dodecyl sulfate−polyacrylamide gel electrophoresis; SSAT, spermine/spermidine N^1-acetyltransferase.

10.1021/bi8009357 CCC: $40.75
Published on Web 08/09/2008

The mouse and human forms of SSAT are nearly identical in sequence, differing in only six amino acids, so all important aspects of enzyme function are likely identical in these two mammalian species. However, the use of the mouse enzyme resulted in previously unobserved crystal forms being obtained, providing new views of the enzyme structure, as well as a first view of a bound polyamine substrate. This new structural information is complemented by kinetic studies using a variety of substrates, as well as site-directed mutations of the enzyme. These results contribute to the basic understanding of how GNAT proteins acetylate polyamines and may assist in the design of molecules that can modulate the activity of SSAT in vivo.

EXPERIMENTAL PROCEDURES

Protein Expression, Purification, and Generation of Site-Directed Mutants. The open reading frame for *Mus musculus* SSAT was amplified by PCR from cDNA using primers designed to introduce *Nde*I and *Bam*HI restriction sites. The amplified DNA was ligated into plasmid pET15b (Novagen). Histidine-tagged SSAT protein was expressed in Rosetta-gami B(DE3) *Escherichia coli* cells (Novagen) grown in Luria broth. Mutants of SSAT were generated by overlap extension PCR using pET15b containing the SSAT DNA as an initial template. The identity of each construct was verified by DNA sequencing.

Expression of wild-type and mutant histidine-tagged SSAT was carried out for 3 h at room temperature after the addition of 0.5 mM IPTG to the cell culture when it had reached an OD_{600} of 0.5. Cells containing the histidine-tagged SSAT were collected by centrifugation, resuspended in 20 mL of PBS buffer per liter of cell culture, and then sonicated on ice. Insoluble material was cleared by centrifugation at 25000*g*. Histidine-tagged SSAT was precipitated from the soluble fraction by the addition of ammonium sulfate to a final concentration of 0.5 g/mL. All subsequent purification steps were carried out at 4 °C. Precipitated protein was resuspended in a buffer containing 100 mM NaCl, 20 mM Tris, and 40 mM imidazole (pH 8.0). Solubilized protein was loaded onto an IMAC column (Amersham), washed, and then eluted with a gradient of up to 500 mM imidazole. Fractions containing histidine-tagged SSAT were identified by SDS−PAGE and pooled. The histidine tag was removed using thrombin, while simultaneously dialyzing into 50 mM NaCl and 20 mM potassium phosphate buffer at pH 7.0. Cleaved and dialyzed SSAT was then loaded onto a Q-Sepharose column (Pharmacia), washed, and eluted using a gradient of up to 1 M NaCl. Fractions containing SSAT were identified by SDS−PAGE, pooled, and dialyzed overnight into 50 mM NaCl and 20 mM potassium phosphate buffer (pH 7.0). Finally, the purified protein was concentrated to 20 mg/mL in the presence 100 μM coenzyme A.

Crystallization and Data Collection. Crystallization screens were performed at 4 °C using the hanging drop vapor diffusion method. Crystals were obtained at pH 5−6.5 over a broad range of precipitant and salt concentrations. There appeared to be a strict requirement for the addition of glycerol (~15%, v/v) and polyamine (~1 mM) for crystallization to occur. Crystals of the binary complex between SSAT and coenzyme A were obtained in 20% PEG 8000, 80 mM sodium acetate, 15% glycerol, 2 mM spermine, 1 mM coenzyme A, and 85 mM sodium cacodylate (pH 6.0). Crystals of the ternary complex, in which electron density for spermine was visible, were obtained by altering the pH and solution contents after the aforementioned crystals were formed. Crystals in 1 μL of mother liquor were transferred to a 10 μL drop containing 20% PEG 8000, 50 mM NaCl, 2 mM spermine, 1 mM coenzyme A, 15% glycerol, and 100 mM bicine buffer (pH 9.0). The crystals were then allowed to soak overnight. All crystals were frozen by being immersed in liquid nitrogen, and diffraction data were collected at 100 K using a MAR CCD detector at the GCPCC beamline at the Center for Advanced Microstructures and Devices (CAMD) in Baton Rouge or using a Rigaku RU-H3R X-ray generator with an R-Axis IV^{++} image plate at the University of Texas.

X-Ray Data Processing and Structure Refinement. Diffraction data were scaled and integrated using HKL2000 (*29*). The structure of SSAT was determined by molecular replacement using MOLREP within the CCP4 program suite (*30*) and a structure of the human form of the protein (PDB entry 2B4D) as a search model. Model refinement and map generation were carried out using CNS (*31*), with manual inspection and modification using O (*32*). Spermine was modeled into coherent electron density after CoA and solvent molecules had been incorporated into the structure; the complex with spermine was then subjected to additional rounds of structure refinement. NCS averaging between the two dimers present in the asymmetric unit was attempted but did not result in an improvement of the calculated electron density maps. The stereochemistry of both SSAT structures was validated using PROCHECK (*33*). The structure was visualized using Pymol (*34*).

Enzyme Activity Assays. A Varian Inova 500 MHz NMR spectrometer was used to monitor the depletion of acetyl-CoA or the generation of acetylpolyamine by measuring the heights of ^{1}H resonances near 1.97 or 2.31 ppm, respectively. The assays were performed at 298 K in 90% H_2O, 10% D_2O, and 100 mM potassium phosphate buffer. The enzyme concentration ranged from 50 nM to 2 μM, depending upon the substrate being tested. Initial rates were determined by measuring NMR peak heights as a function of time. Typically, seven polyamine concentrations, ranging from 1 to 20 mM, were used in assaying the enzyme activity at a variety of pH values. k_{cat} and, under favorable circumstances, K_m were determined by fitting the rate data to the Michaelis−Menten equation using DYNAFIT. Control reactions were performed in the absence of the enzyme, over a broad range of solution conditions, to ensure that competing chemical reactions did not distort the observed kinetic data. Data for the spermine diacetylation assay were processed using NMRPipe (*35*); peak heights were measured using SPARKY (*36*), and rate constants for first and second diacetylation steps were fit using DYNAFIT (*37*).

RESULTS

Structure of the Binary Complex. Recombinant SSAT from mouse was cocrystallized as a binary complex with CoA, yielding crystals that diffracted X-rays to 2.1 Å resolution (Table 1). The asymmetric unit of the crystal was found to contain four protein molecules (arranged as two dimers) and four molecules of bound CoA. The four protein molecules

Table 1: Summary of Crystallographic and Structural Statistics for SSAT[a]

	SSAT with coenzyme A	SSAT with coenzyme A and spermine
PDB entry	3BJ7	3BJ8
space group	$P2_12_12_1$	$P2_12_12_1$
unit cell dimensions (Å)	$a = 76.86$	$a = 77.25$
	$b = 97.19$	$b = 97.12$
	$c = 105.70$	$c = 105.50$
no. of protein molecules per asymmetric unit	4	4
Matthews coefficient (Å^3/Da)	2.35	2.36
maximum resolution (Å)	2.10	2.30
data collection wavelength (Å)	1.38	1.54
total no. of reflections	209333	122476
no. of unique reflections	46525	35462
R_{sym} (%)	4.8 (38.9)	8.1 (46.6)
completeness (%)	96.8 (76.7)	98.0 (98.3)
I/σ	26.3 (2.7)	23.4 (3.9)
resolution range for refinement (Å)	32.4−2.1	39.0−2.3
R_{work} (%)	23.2 (31.5)	23.1 (29.9)
R_{free} (%)	29.4 (37.7)	28.2 (37.3)
no. of protein atoms	5336	5330
no. of water molecules	331	213
no. of ligand atoms	192	206
average B-factor (Å^2)		
protein	34.7	36.3
solvent	35.8	39.3
coenzyme A	41.6	46.4
spermine	NA	46.8
rmsd from ideal geometry, covalent bonds (Å)	0.007	0.008
rmsd from ideal geometry, covalent angles (deg)	1.24	1.27
Ramachandran plot		
residues in favored regions	93.2%	93.3%
residues in allowed regions	6.8%	6.3%
residues in generously allowed regions	0.0%	0.4%
residues in disallowed regions	0.0%	0.0%

[a] Values in parentheses refer to the highest-resolution shell (10%) of the X-ray data. The data for the binary complex between SSAT and coenzyme A were collected at 100 K using a synchrotron X-ray source (CAMD), and data for the ternary complex containing SSAT, coenzyme A, and spermine were collected at 100 K using a home source X-ray generator equipped with a rotating copper anode.

were similar in structure; however, there were some small differences, probably a consequence of the packing within the crystal. For example, in one of the four protein molecules, residues 130−155 were not well-ordered. The differences between the four protein molecules in the asymmetric unit were significant enough such that noncrystallographic symmetry averaging did not improve the quality of the structure; the molecules were therefore refined independently (Table 1). All amino acids were visible in at least one of the protein molecules, with the exceptions of the first two amino acids at the N-terminus, and the last three amino acids at the C-terminus.

Mouse SSAT contains the mixed α/β-architecture that is characteristic of the GNAT superfamily. Specifically, it is a homodimer with a β-sheet core, where the β-sheet is built from residues contributed by each monomer (Figure 1). In binding of CoA, the mouse SSAT exhibits the conserved features seen in other GNAT proteins (*22*). The CoA is bound in a cleft between alpha4, the C-terminal end of beta4 and the N-terminal end of alpha3, with the sulfhydryl end of CoA located in the splay between β4 and β5. The most conserved interaction between the protein and CoA involves the "P-loop", consisting of residues 100−107, and containing the conserved GXGXG motif (*38*) (Figure 2). The glycines within the P-loop permit the protein backbone to adopt a conformation in which a water molecule is coordinated to the carbonyl oxygen of Tyr100 and the amide protons of Phe103 and Ile105. This water molecule, along with backbone atoms of residues Gly102, Gly104, Gly106, and Ser107, forms a network of hydrogen bonds with the pyrophosphate group of CoA. The side chain of Asn133, which is also conserved among the GNAT acetyltransferases, is hydrogen-bonded to the carbonyl oxygen of CoA closest to its sulfhydryl group. A bend is present in the CoA molecule, located between the two peptide bonds in the pantothenate unit, which has been observed in complexes of other GNAT proteins (*22*).

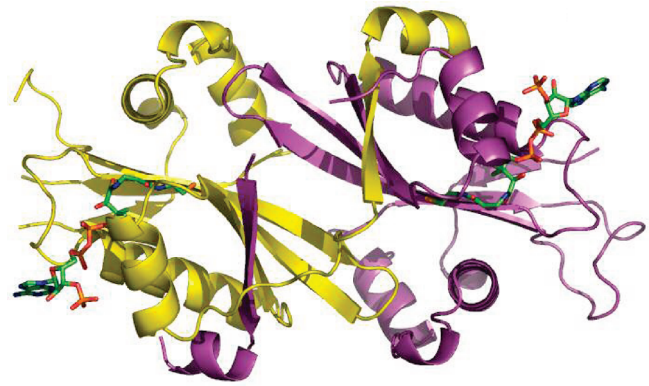

FIGURE 1: Ribbon diagram of the mouse SSAT−CoA binary complex, with the two protein molecules of the dimer shown in different colors. The sulfhydryl group of CoA is located near the enzyme active site, while the adenosine ring is relatively exposed.

Ternary Complex with Bound Spermine. The ternary complex of SSAT, CoA, and spermine was reconstituted by altering the solution conditions of preformed crystals of the binary complex. CoA, instead of acetyl-CoA, was used in the ternary complex to prevent turnover of the bound polyamine substrate. Clear electron density for spermine could be observed in one of the four potential binding sites within the asymmetric unit of the crystal. Both of the dimers in the asymmetric unit were in similar conformations, despite the appearance of bound spermine in only one of the two dimers. This partial occupancy of spermine binding sites may be a consequence of crystal packing and is reminiscent of the ternary complex of human SSAT with the inhibitor BE-3-3-3, where the inhibitor was observed in only one of the two possible binding sites of an SSAT dimer (*24*).

Binding of spermine by SSAT involves a combination of hydrophobic and polar interactions, the latter of which are mostly mediated by water molecules. The hydrophobic contacts involve the side chains of Leu128, Leu156, and Trp154′ (where the prime denotes a residue in the adjoining SSAT monomer). The N1 amine of the bound spermine is located in the enzyme active site, very near the position occupied by the sulfhydryl group of CoA in the binary complex. An ordered water molecule near the enzyme active site connects this amine with the backbone amine of Leu128 and the backbone carbonyl of Leu91 (Figure 3). This places the water molecule at the base of the splay between β4 and β5, which is a conserved structural feature of GNAT proteins. The water molecule also appears to connect the N1 amine of spermine to the side chain of Glu92,

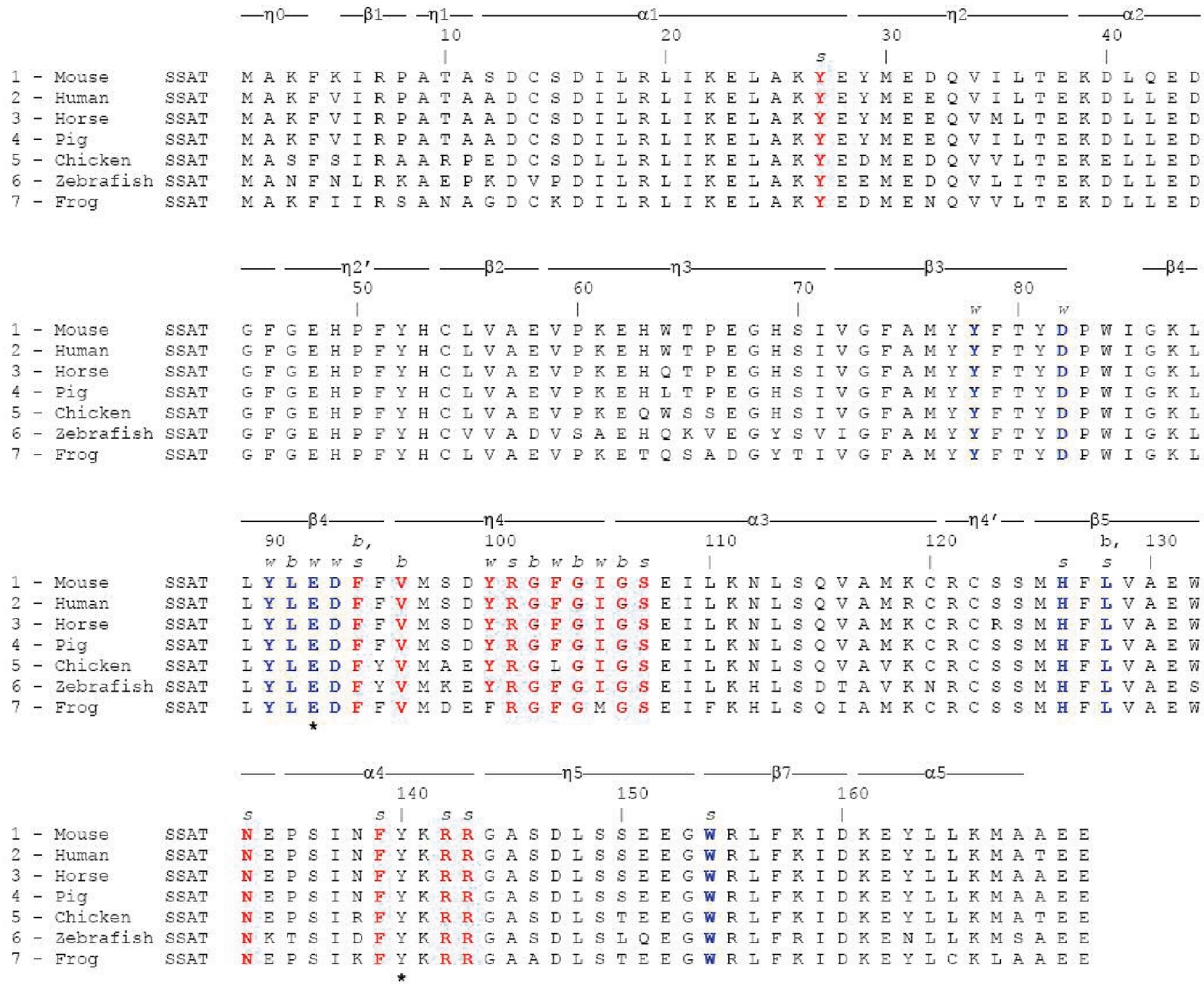

FIGURE 2: Sequence alignment showing the similarity between mouse and human SSAT, along with five putative SSATs from various higher organisms. Conserved residues that interact with spermine are colored blue, and those that interact with coenzyme A are colored red. Italicized characters above the mouse sequence denote intermolecular contacts that are mediated by the backbone of an amino acid (*b*), the side chain of an amino acid (*s*), or an associated water molecule (*w*). The two proposed catalytic residues, Glu92 and Tyr140, are denoted with an asterisk. Strands are numbered to be consistent with structures of SSAT from other species; the region previously identified as β6 was not well-ordered in the mouse structure and is instead labeled η5.

through the action of another bridging water molecule. Together, these two water molecules form a proton wire in the enzyme active site (*22, 23, 25, 28*). The N4 amine of spermine is bound to the side chains of Glu92 and Asp93 by hydrogen bonds with a third bridging water molecule, while a fourth water molecule bridges the contact between the N9 amine and the side chains of Asp82′ and Glu92. A hydrogen bond links the N12 amine of spermine to the side chain of His126′. The contacts between the mouse SSAT, the bound spermine substrate, and bridging water molecules are summarized schematically in Figure 3. This work provides the first crystallographic view of a bound polyamine substrate of SSAT, as opposed to bound inhibitors, as had been previously described (*24, 28*).

Structural Plasticity near the Enzyme Active Site. Binding of spermine resulted in changes in the structure of the protein, and displacement of the pantothenate group of CoA from the enzyme active site (Figure 4), although the pyrophosphate of CoA maintains the conserved interaction with the P-loop. In the protein, the N-terminal end of helix α4 and the loop connecting it to strand β5 were displaced by approximately 2 Å, compared to their locations in the binary complex. This expansion of the protein structure may be a necessary response to accommodate spermine binding. The location of the bound spermine, with its N1 amine near the position observed for the sulfur of CoA in the binary complex, may provide an explanation for why two CoA molecules (one from each dimer) are displaced from the enzyme active site in the ternary complex. There also appears to be a disulfide linkage between the two displaced CoA molecules; the other two CoA molecules in the asymmetric unit are somewhat disordered, although the electron density map suggests that they are in a conformation similar to that seen in the binary complex. A similarly displaced CoA was observed in the structure of the ternary complex of human SSAT with a polyamine analogue (*24*).

Comparison of Spermine and Inhibitor Binding. Although there are some similarities between how SSAT binds spermine and how it binds inhibitors, there are also significant differences. Binding of spermine uses several of the same residues that are involved in binding the inhibitor N^1,N^{11}-bis(ethyl)norspermine (BE-3-3-3) (*24*), although spermine protrudes significantly further into the active site than BE-3-3-3 (Figure 5). As in the binding of BE-3-3-3, spermine was observed in only one of the two possible binding sites in the dimer; this differs from the structure of the human SSAT with the bisubstrate analogue N^1-spermine-acetyl-CoA,

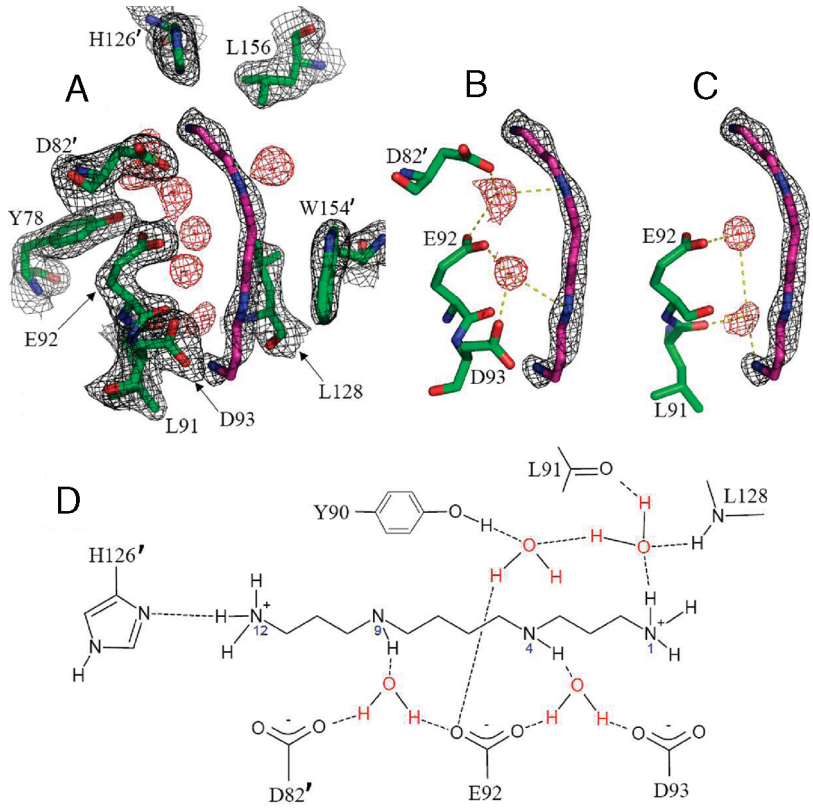

FIGURE 3: Electron density maps showing bound spermine in the SSAT−CoA−spermine ternary complex, contoured at 1.5σ. To minimize model bias, the map was generated piecewise by systematically deleting small regions of the model and then performing simulated annealing before calculating an electron density map within the deleted region. (A) Section of the electron density map showing all residues involved in spermine binding. (B) Water-mediated contacts between the protein and the N4 and N9 atoms of spermine. (C) Two water molecules form a proton wire between N1 of spermine and Glu92. (D) Schematic diagram showing the hydrogen-bonding and water-mediated contacts between SSAT and spermine.

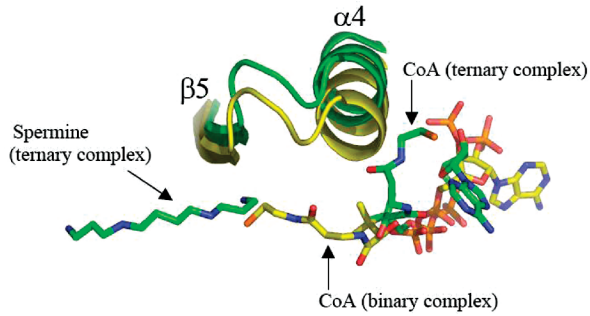

FIGURE 4: Superposition of mouse SSAT as observed in the binary complex with CoA (yellow) and as a ternary complex with CoA and spermine (green). Introduction of spermine resulted in displacement of CoA from the enzyme active site.

where both binding sites could be occupied simultaneously by the bisubstrate (*28*). In the case of the bisubstrate analogue, N12 of the polyamine moiety was located near Glu28, on an exposed surface loop, while in the work presented here, the analogous nitrogen in spermine is linked to His126′ by a hydrogen bond. A comparison of the binding of spermine, BE-3-3-3, and the bisubstrate analogue is shown in Figure 5.

Acetylation of Polyamines by SSAT. Enzyme activity assays were combined with the structural results to provide insights into the important determinants of substrate specificity, as well as the enzyme mechanism. ^{1}H NMR spectroscopy was used to evaluate the activity of mouse SSAT toward a variety of potential substrates (Table 2 and Figures 6 and S1−S3). This NMR-based assay is advantageous in that it can be used to simultaneously monitor the appearance of products and the disappearance of reactants, while identifying the products formed. In addition, the NMR assay permits the integrity of the acetyl-CoA substrate to be monitored so that the kinetics results are not distorted by the degradation of this substrate during the activity assays. A limitation of the NMR assay is its relatively low sensitivity; the assay is best applied using substrate concentrations in the millimolar range.

The ability of recombinant mouse SSAT to acetylate spermine, spermidine, and related substrates was tested at pH 8.5 (Table 2), using typically 1−2 mM acetyl-CoA and 1−16 mM polyamine. The reaction rate did not significantly depend on polyamine or acetyl CoA concentration in this range, suggesting that the enzyme was saturated under these conditions (Figure S4). On the basis of k_{cat}, the enzyme was found to be most active with spermidine as a substrate, approximately 9-fold less active toward spermine, and approximately 4−5-fold less active when diethylenetriamine and 1,3-diaminopropane were used as substrates (Table 2). All substrates for which there was measurable activity were acetylated at a primary amine. These results for mouse SSAT are similar to those reported for the enzyme isolated from rat liver (*11*) and recombinant human SSAT (*28*), for which the activity assays were performed using other methods. Our preparation of mouse SSAT did not have a detectable ability to acetylate cadaverine, putrescine, lysine, thialysine, or amantadine; the result for this latter substrate differs from a previous report (*39*).

The NMR-based activity assay is well suited for detecting additional sites of acetylation of the polyamine, after the

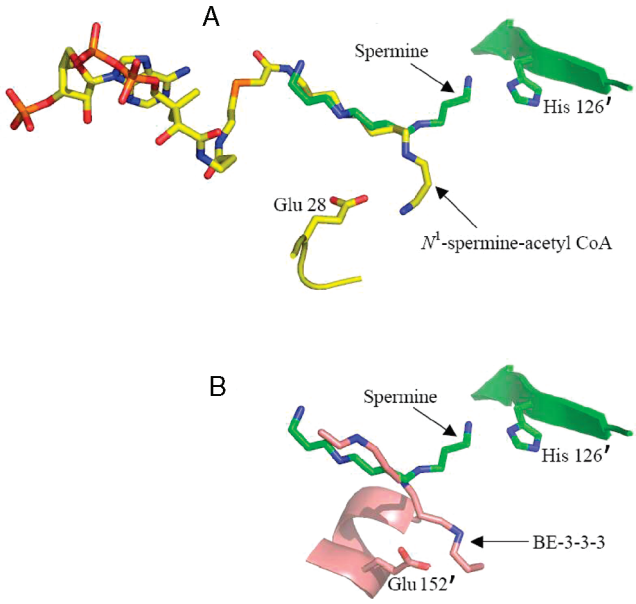

FIGURE 5: (A) Diagram comparing the binding of spermine (observed in this work) with the binding of the bisubstrate analogue N^1-spermine-acetyl-CoA (*28*). The bisubstrate analogue and Glu28 are from the human SSAT (PDB entry 2JEV) and are colored yellow; spermine and His126′ are from the mouse SSAT and are colored green. A prime indicates the amino acid belongs to the second protein subunit within the dimer. (B) Diagram comparing the binding of spermine with the binding of the inhibitor N^1,N^{11}-bis(ethyl)norspermine (BE-3-3-3) (*24*). The BE-3-3-3 molecule and Glu152′ are from the human SSAT (PDB entry 2B4B) and are colored purple; the spermine molecule and His126′ are from the mouse SSAT. The mouse and human forms of SSAT differ by only six amino acids and are therefore likely to bind spermine, BE-3-3-3, and N^1-spermine-acetyl-CoA similarly.

Table 2: Rates of SSAT-Catalyzed Acetylation of Various Polyamine Substrates at pH 8.5 and 25 °C[a]

substrate	k_{cat} (s^{-1})
spermidine	12.7 ± 0.3
spermine N^1-acetylspermine	1.4 ± 0.1
diethylenetriamine	3.7 ± 0.2
1,3-diaminopropane	2.4 ± 0.1
N-methyl-1,3-diaminopropane	0.7 ± 0.04
putrescine	ND[b]
cadaverine	ND[b]
lysine	ND[b]
thialysine	ND[b]
amantadine	ND[b]

[a] Experiments were performed using a range of substrate concentrations to verify that the enzyme was saturated under the assay conditions, allowing determination of k_{cat} from the initial rate of reaction. In the cases of spermine and N^1-acetylspermine, k_{cat} was determined using the data described in Figure 6 and DYNAFIT, due to the multistep nature of the reaction. Chemical structures of these substrates are shown in Figure S1 of the Supporting Information. [b] No activity was detected.

substrate had been acetylated at a first position. In the case of spermine, NMR spectra showed the appearance of a product that is acetylated in a second position (the N12 amine) after the appearance of the initial product acetylated at N1 (Figure 6). In this multistep reaction, the substrate for the second acetylation was generated in situ as the product of the first acetylation. The NMR method was able to resolve separate signals for both the mono- and diacetylated spermine (Figure 6) so that the concentration of each reactant and product could be monitored simultaneously. The kinetics of the multistep reaction were modeled using DYNAFIT (*37*)

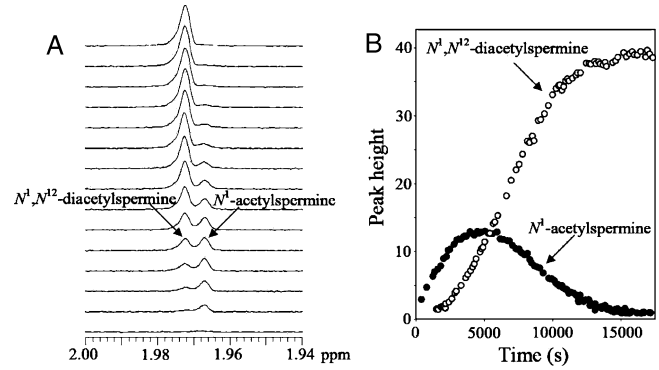

FIGURE 6: Both of the aminopropyl moieties in spermine can be acetylated by SSAT, even when one has already been acetylated. (A) ^{1}H NMR spectra showing the production and eventual consumption of N^1-acetylspermine, shown at 20 min time intervals. (B) ^{1}H NMR peak heights of N^1-acetylspermine and N^1,N^{12}-diacetylspermine plotted as a function of time. The initial concentrations of spermine and acetyl-CoA were 1 and 3 mM, respectively, with an enzyme concentration of 100 nM at pH 8.5.

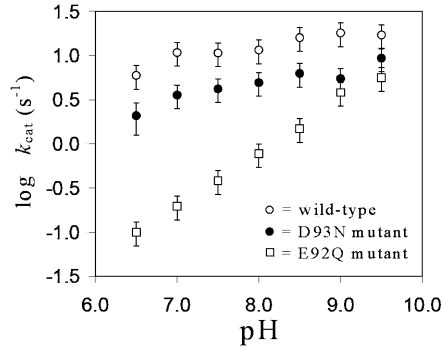

FIGURE 7: pH dependence of SSAT activity. Initial reaction rates were measured using at least seven different starting concentrations of spermidine (ranging from 2 to 20 mM); the rates were then fit to the Michaelis−Menten equation to determine k_{cat} and, when possible, K_m. A saturating concentration of acetyl-CoA (2 mM) was used over the entire pH range studied. ^{1}H NMR spectra were used to verify that the protein was folded at each pH extreme.

to yield rates for each spermine acetylation, using data collected from a single reaction mixture. Results show that spermine and N^1-acetylspermine are comparable as substrates for the recombinant mouse SSAT (Table 2), which is consistent with a previous result reported for the enzyme isolated from rat liver and assayed using a different method (*11*).

pH Dependence of SSAT Activity. We investigated the pH dependence of the enzyme activity to shed further light on the enzyme mechanism. Spermidine was used as a model substrate in evaluating pH effects, since it is an excellent substrate for SSAT, its reaction kinetics are not complicated by multiple acetylation steps (as in the case of spermine), and it has been previously used in an investigation of the human enzyme (*28*). With spermidine as a substrate, the mouse SSAT was found to be most active between pH 8.5 and 9.5 (Figure 7). The catalytic ability of the enzyme decreased steadily below the optimal pH; the value for k_{cat} at pH 6.0 was approximately one-third of that at pH 8.5. Between pH 7.5 and 9.5, the enzyme was found to be saturated with spermidine over the range of concentrations accessible in the NMR assay (Figure S4). However, at lower pH values, the reaction rate was dependent on spermidine concentration so that the NMR assay was capable of

measuring an approximate K_m of 20 mM at pH 6 (Figure S4). The relatively low k_{cat} and substrate binding affinity made it difficult to measure the activity of the enzyme below pH 6 using the NMR-based assay. These results are generally similar to those reported for the human SSAT when using an entirely different assay method; however, there are some differences. For example, in the case of the human SSAT, a more pronounced reduction in k_{cat} was observed below pH 8.0.

Mutational Analysis of Mouse SSAT. Site-directed mutants were prepared for the purpose of testing the roles of Glu92 and Asp93 in enzymatic function; both of these residues are located near the enzyme active site and make contacts with the bound spermine in the crystal structure of the ternary complex (Figure 3). Mutation of Glu92 to glutamine resulted in an enzyme with reduced activity, with a pH dependence distinctly different from that found in the wild-type SSAT (Figure 7). In the E92Q mutant, k_{cat} increased steadily with increasing pH, and unlike the wild-type enzyme, the activity did not reach a plateau above pH 8.5. Interestingly, this mutant exhibited a k_{cat} value that was less than 5% of that of the wild-type enzyme at physiological pH (Figure 7). The E92Q mutation also increased K_m to approximately 5 mM at pH 8.5. Mutation of Asp93 to asparagine reduced k_{cat} by approximately 2-fold and increased K_m to approximately 0.5 mM at pH 8.5 (Figure 7). However, unlike that of the E92Q mutant, the pH dependence of k_{cat} for the D93N mutant was similar to that found in the wild-type enzyme. In the case of both mutants, there was a significant increase in K_m when the pH was lowered below 7.0; this is similar to the wild-type enzyme, where K_m increased to approximately 20 mM at pH 6.0.

DISCUSSION

The crystal structure of the ternary complex of mouse SSAT, CoA, and spermine provides the first view of the binding of a polyamine substrate by an acetyltransferase. An examination of structures in the Protein Data Bank provides only one other example of spermine bound in the active site of an enzyme. Yeast Fms1, a spermine oxidase, makes both hydrophobic and polar contacts with bound spermine (*40*). However, unlike SSAT, the polar contacts in Fms1 do not rely on associated water molecules. The use of water molecules to mediate the interactions between SSAT and spermine may reflect a need for the enzyme to not bind its substrates too tightly, since the SSAT reaction product, unlike that of Fms1, still possesses many of the features recognized in the initial substrate.

In this work, the structural model for spermine binding is complemented with kinetics data involving multiple substrates, site-directed mutants, and pH−activity profiles. Taken together, these results can be considered in the context of current models for the enzyme mechanism (Figure 8). The GNAT proteins typically catalyze acetyl transfer reactions through the use of general acid−base catalysis, where a catalytic base deprotonates the N1 amine of a polyamine and a catalytic acid protonates the sulfur of acetyl CoA. The ternary and binary complexes presented here each possess a tyrosine residue (Tyr140) that is positioned well to fulfill the role of the catalytic acid. Consistent with this hypothesis, and with a previous study of human SSAT (*24*), mutation

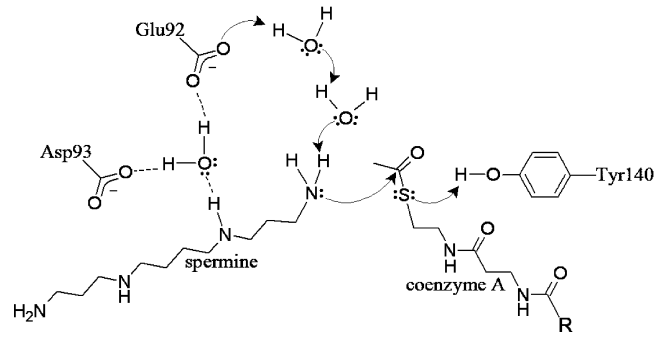

FIGURE 8: Proposed enzyme mechanism, derived from the structural and kinetic results. The N1 amine of the polyamine substrate is deprotonated by Glu92, and the sulfur of acetyl-CoA is protonated by Tyr140. The crystal structure suggests that associated water molecules play a central role in substrate binding and catalysis.

of this tyrosine led to a large decrease in enzyme activity (data not shown). The identity of the catalytic base is less apparent; previous work has suggested Glu28 (*24, 41*), although more recent studies have implicated Glu92 through the use of associated water molecules (*28*). The structure of the ternary complex shows that Glu92 is connected to the N1 amine of spermine by way of a proton wire, formed by two water molecules (Figure 3D). The water molecules in this wire could shuttle a proton from N1 to the side chain of Glu92, thus allowing the glutamate to function as a catalytic base.

This work describes the first site-directed mutant of Glu92, where mutation to glutamine was found to significantly decrease k_{cat}, and increase K_m. These results are consistent with the position of Glu92 in the structure of the ternary complex, where it is well-positioned to participate in substrate binding and catalysis. Additionally, this mutation altered the pH dependence of the enzyme, with the greatest decrease in k_{cat} occurring at the low end of the investigated pH range (Figure 7). ^{1}H NMR spectra were used to ensure that mutagenized proteins were folded over the pH range studied; it is therefore unlikely that these pH effects arise from protein denaturation. One possible explanation for the pH dependence of the E92Q mutant is that the residue is unable to accept a proton, and hydroxide ions in solution must instead fulfill the role of proton acceptor. Consistent with this hypothesis, ordered water molecules in the ternary complex can be seen linking the proton wire to the exterior of the protein. The NMR-based activity assay was unable to accurately measure the wild-type and mutant enzyme activities below pH 6, due to the reduction in substrate binding and low k_{cat}. In the case of the wild-type enzyme, this prevented identification of a pH range where log k_{cat} is linearly dependent on pH; therefore, the titration of the catalytic base in the wild-type protein was not oberved. However, the significant difference between the pH dependence of wild-type and mutant forms of SSAT is consistent with Glu92 fulfilling the role of the catalytic base.

Mutation of Asp93 also led to a reduction in enzyme activity. However, it seems unlikely that this residue is directly involved in catalysis, since k_{cat} is reduced by a factor of only 2 when it is replaced with asparagine. The location of Asp93 within the structure suggests that it is likely to exert some effect on the network of water molecules that form the proton wire, which could provide an explanation for the observed reduction in k_{cat}. Another possible explana-

tion for the reduced activity of the Asp93 mutant involves the residue's proximity to Glu92. Both Asp93 and Glu92 are located on the β-bulge of β4, which serves to position their side chain carboxylates on the same face of the central β-sheet. The relative positions of these two conserved functional groups could enhance the ability of Glu92 to serve as a proton acceptor at physiological pH.

In conclusion, the crystal structure of SSAT in complex with spermine shows how the enzyme specifically recognizes one of its natural substrates, and the accompanying kinetics data provide insights into the enzyme mechanism. These and other studies will increase the likelihood of designing molecules that can selectively interact with SSAT; an ability to specifically target SSAT in vivo could open the door to new strategies for treating polyamine-related diseases.

SUPPORTING INFORMATION AVAILABLE

Structures of the polyamines used in SSAT activity assays, sample ^{1}H NMR spectra, and additional kinetics data. This material is available free of charge via the Internet at http://pubs.acs.org.

REFERENCES

1. Tabor, C. W., and Tabor, H. (1976) 1,4-Diaminobutane (putrescine), spermidine, and spermine. *Annu. Rev. Biochem. 45*, 285–306.
2. Herbst, E. J., and Elliot, Q. D. (1981) Role of polyamines in HeLa cell proliferation. *Med. Biol. 59*, 410–416.
3. McCormack, S. A., and Johnson, L. R. (2001) Polyamines and cell migration. *J. Physiol. Pharmacol. 52*, 327–349.
4. Manni, A. (2002) Polyamine involvement in breast cancer phenotype. *In Vivo 16*, 493–500.
5. Schipper, R. G., Romijn, J. C., Cuijpers, V. M., and Verhofstad, A. A. (2003) Polyamines and prostatic cancer. *Biochem. Soc. Trans. 31*, 375–380.
6. Milovic, V., and Turchanowa, L. (2003) Polyamines and colon cancer. *Biochem. Soc. Trans. 31*, 381–383.
7. Casero, R. A., and Marton, L. J. (2007) Targeting polyamine metabolism and function in cancer and other hyperproliferative diseases. *Nat. Rev. Drug Discovery 6*, 373–390.
8. Seiler, N. (2003) Thirty years of polyamine-related approaches to cancer therapy. Retrospect and prospect. Part 1. Selective enzyme inhibitors. *Curr. Drug Targets 4*, 537–564.
9. Seiler, N. (2003) Thirty years of polyamine-related approaches to cancer therapy. Retrospect and prospect. Part 2. Structural analogues and derivatives. *Curr. Drug Targets 4*, 565–585.
10. Wallace, H. M. (2007) Targeting polyamine metabolism: A viable therapeutic/preventative solution for cancer? *Expert Opin. Pharmacother. 8*, 2109–2116.
11. Della Ragione, F., and Pegg, A. E. (1983) Studies of the specificity and kinetics of rat liver spermidine/spermine N^1-acetyltransferase. *Biochem. J. 213*, 701–706.
12. Fogel-Petrovic, M., Vujcic, S., Brown, P. J., Haddox, M. K., and Porter, C. W. (1996) Effects of polyamines, polyamine analogs, and inhibitors of protein synthesis on spermidine-spermine N 1-acetyltransferase gene expression. *Biochemistry 35*, 14436–14444.
13. Aubel, C., Chabanon, H., Carraro, V., Wallace, H. M., and Brachet, P. (2003) Expression of spermidine/spermine N^1-acetyltransferase in HeLa cells is regulated by amino acid sufficiency. *Int. J. Biochem. Cell Biol. 35*, 1388–1398.
14. Hyvönen, M. T., Uimari, A., Keinänen, T. A., Heikkinen, S., Pellinen, R., Wahlfors, T., Korhonen, A., Närvänen, A., Wahlfors, J., Alhonen, L., and Jänne, J. (2006) Polyamine-regulated unproductive splicing and translation of spermidine/spermine N^1-acetyltransferase. *RNA 12*, 1569–1582.
15. Butcher, N. J., Broadhurst, G. M., and Minchin, R. F. (2007) Polyamine-dependent regulation of spermidine-spermine N^1-acetyltransferase mRNA translation. *J. Biol. Chem. 282*, 28530–28539.
16. Wallace, H. M., Fraser, A. V., and Hughes, A. (2003) A perspective of polyamine metabolism. *Biochem. J. 376*, 1–14.
17. Casero, R. A., and Pegg, A. E. (1993) Spermidine/spermine N^1-acetyltransferase: The turning point in polyamine metabolism. *FASEB Lett. 7*, 653–661.
18. Seiler, N. (1995) Polyamine oxidase, properties and functions. *Prog. Brain Res. 106*, 333–344.
19. Vujcic, S., Liang, P., Diegelman, P., Kramer, D. L., and Porter, C. W. (2003) Genomic identification and biochemical characterization of the mammalian polyamine oxidase involved in polyamine back-conversion. *Biochem. J. 370*, 19–28.
20. Vetting, M. W., S de Carvalho, L. P., Yu, M., Hegde, S. S., Magnet, S., Roderick, S. L., and Blanchard, J. S. (2005) Structure and functions of the GNAT superfamily of acetyltransferases. *Arch. Biochem. Biophys. 433*, 212–226.
21. Angus-Hill, M. L., Dutnall, R. N., Tafrov, S. T., Sternglanz, R., and Ramakrishnan, V. (1999) Crystal structure of the histone acetyltransferase Hpa2: A tetrameric member of the Gcn5-related *N*-acetyltransferase superfamily. *J. Mol. Biol. 294*, 1311–1325.
22. Dyda, F., Klein, D. C., and Hickman, A. B. (2000) GCN5-related *N*-acetyltransferases: A structural overview. *Annu. Rev. Biophys. Biomol. Struct. 29*, 81–103.
23. Scheibner, K. A., De Angelis, J., Burley, S. K., and Cole, P. A. (2002) Investigation of the roles of catalytic residues in serotonin *N*-acetyltransferase. *J. Biol. Chem. 277*, 18118–18126.
24. Bewley, M. C., Graziano, V., Jiang, J., Matz, E., Studier, F. W., Pegg, A. E., Coleman, C. S., and Flanagan, J. M. (2007) Structures of wild-type and mutant human spermidine/spermine N^1-acetyltransferase, a potential therapeutic drug target. *Proc. Natl. Acad. Sci. U.S.A. 103*, 2063–2068.
25. Hickman, A. B., Namboodiri, M. A., Klein, D. C., and Dyda, F. (1999) The structural basis of ordered substrate binding by serotonin *N*-acetyltransferase: Enzyme complex at 1.8 Å resolution with a bisubstrate analog. *Cell 97*, 361–369.
26. Tanner, K. G., Trievel, R. C., Kuo, M. H., Howard, R. M., Berger, S. L., Allis, C. D., Marmorstein, R., and Denu, J. M. (1999) Catalytic mechanism and function of invariant glutamic acid 173 from the histone acetyltransferase GCN5 transcriptional coactivator. *J. Biol. Chem. 274*, 18157–18160.
27. Hung, M. N., Rangarajan, E., Munger, C., Nadeau, G., Sulea, T., and Matte, A. (2006) Crystal structure of TDP-fucosamine acetyltransferase (WecD) from *Escherichia coli*, an enzyme required for enterobacterial common antigen synthesis. *J. Bacteriol. 188*, 5606–5617.
28. Hegde, S. S., Chandler, J., Vetting, M. W., Yu, M., and Blanchard, J. S. (2007) Mechanistic and structural analysis of human spermidine/spermine N^1-acetyltransferase. *Biochemistry 46*, 7187–7195.
29. Otwinowski, Z., and Minor, W. (1997) Processing of X-ray Diffraction Data Collected in Oscillation Mode. *Methods Enzymol. 276*, 307–326.
30. Vagin, A. A., and Teplyakov, A. (1997) Molrep: An automated program for molecular replacement. *J. Appl. Crystallogr. 30*, 1022–1025.
31. Brunger, A. T., Adams, P. D., Clore, G. M., Delano, W. L., Gros, P., Grosse-Kunstleve, R. W., Jiang, J. S., Kuszewski, J., Nilges, M., Pannu, N. S., Read, R. J., Rice, L. M., Simonson, T., and Warren, G. L. (1998) Crystallography & NMR system: A new software system for macromolecular structure determination. *Acta Crystallogr. D54*, 905–921.
32. Jones, T. A., Zou, J. Y., Cowan, S. W., and Kjeldgaard, M. (1991) Improved methods for the building of protein models in electron density maps and the location of errors in these models. *Acta Crystallogr. 47*, 110–119.
33. Laskowski, R. A., MacArthur, M. W., Moss, D. S., and Thornton, J. M. (1993) PROCHECK: A program to check the stereochemical quality of protein structure. *J. Appl. Crystallogr. 26*, 283–291.
34. DeLano, W. L. (2002) *The PyMOL Molecular Graphics System*, DeLano Scientific, San Carlos, CA.
35. Delaglio, F., Grzesiek, S., Vuister, G. W., Zhu, G., Pfeifer, J., and Bax, A. (1995) NMRPipe: A multidimensional spectral processing system based on UNIX pipes. *J. Biomol. NMR 6*, 277–293.
36. Goddard, T. D., and Kneller, D. G. (2006) SPARKY 3, University of California, San Francisco.
37. Kuzmic, P. (1996) Program DYNAFIT for the Analysis of Enzyme Kinetic Data: Application to HIV Proteinase. *Anal. Biochem. 237*, 260–273.
38. Lu, L., Berkey, K. A., and Casero, R. A. (1996) RGFGIGS is an amino acid sequence required for acetyl coenzyme A binding and activity of human spermidine/spermine N^1-acetyltransferase. *J. Biol. Chem. 271*, 18920–18924.

39. Bras, A. P., Jänne, J., Porter, C. W., and Sitar, D. S. (2001) Spermidine/spermine N^1-acetyltransferase catalyzes amantadine acetylation. *Drug Metab. Dispos. 29*, 676–680.
40. Huang, Q., Liu, Q., and Hao, Q. (2005) Crystal structures of Fms1 and its complex with spermine reveal substrate specificity. *J. Mol. Biol. 348*, 951–959.
41. Coleman, C. S., Huang, H., and Pegg, A. E. (1995) Role of the carboxyl terminal MATEE sequence of spermidine/spermine N^1-acetyltransferase in the activity and stabilization by the polyamine analog N^1,N^{12}-bis(ethyl)spermine. *Biochemistry 34*, 13423–13430.

BI8009357